# Chapter 4
# Satellite Instrumentation and Technique for Oil Pollution Monitoring of the Seas


**Andrey G. Kostianoy and Olga Yu. Lavrova**

**Abstract** The chapter provides a brief overview of satellite instrumentation, techniques and methods for oil spill detection on the sea surface. Monitoring of oil pollution from space is usually carried out using the synthetic aperture radars (SAR) and advanced synthetic aperture radars (ASAR) installed on satellites launched in different years by USA, ESA, USSR, Japan, Canada, Germany, and Italy. The first SAR system was installed on the SEASAT satellite launched on 27 June 1978, and since that time SAR systems showed their efficiency in oil spill detection on the sea surface. As any remote, in-situ or laboratory method, SAR remote sensing has a set of advantages (wide swath, all weather, day/night, daily periodicity, etc.) as well as disadvantages which include look-alikes caused by natural oceanic and atmospheric phenomena and processes, which need to be discriminated from oil pollution. Application of the SAR systems is illustrated by several examples of oil spill detection in different parts of the World Ocean and inland seas. Discussion of the assessment of total volume of oil pollution for the Baltic and Mediterranean seas shows that this is a difficult task and we still do not know real values of oil pollution of the marine environment. Development of scientific foundations and methodology for the quantitative assessment of environmental state of marine areas and of total amount of oil pollution of the World Ocean and inland seas is extremely urgent. Excessive human activity on the sea, including shipping, exploration and development of off-shore oil and gas reserves, construction and operation of underwater pipelines, platforms, terminals, storage facilities, ports, etc., entail very high risk of oil pollution in many sea areas.

A. G. Kostianoy (✉)
P.P. Shirshov Institute of Oceanology, Russian Academy of Sciences, 36, Nakhimovsky Pr, Moscow 117997, Russian Federation
e-mail: kostianoy@gmail.com

S.Yu. Witte Moscow University, 12, 2nd Kozhukhovksy Per., Bldg. 1, Moscow 115432, Russian Federation

A. G. Kostianoy · O. Yu. Lavrova
Space Research Institute, Russian Academy of Sciences, 84/32, Profsoyuznaya Str, Moscow 117997, Russia
e-mail: olavrova@iki.rssi.ru



A. Di Mauro et al. (eds.), *Instrumentation and Measurement Technologies for Water Cycle Management*, Springer Water, https://doi.org/10.1007/978-3-031-08262-7_4

**Keywords** Satellite instrumentation · Techniques · Monitoring · World Ocean · Seas · Oil pollution · Oil spills · SAR · Aerial surveillance

## 4.1 Introduction

In recent years, remote sensing of the Earth from space has undergone rapid development, which is associated with the following three factors: firstly, this field of space technologies is the second after space communications, where significant commercial potential is seen; secondly, the problem of anthropogenic impact on the World Ocean requires a global network for monitoring the ocean surface and the near-surface layer of the atmosphere, a key element of which is space surveillance; and in the third, various satellite information about the state of the World Ocean, the atmosphere and land is the most important source of data for global and regional climate research. In many cases, remote sensing data on water pollution and quality is a single source of valuable information even if this is not a direct in-situ method of measurements. Direct and indirect (remote sensing) methods of measurements of water quality have their own instrumentation and techniques, as well as advantages and disadvantages characteristic for them.

It is of urgent necessity to develop the science basis and techniques for quantitative estimation of the state of marine environment. Here, the crucial point is evaluating pollution and metocean dynamics through a comprehensive analysis of satellite data. Certain inland (Mediterranean, Red, Baltic, Black, Caspian) and marginal (North, Barents, Kara) seas and large gulfs (Persian, Mexico, Guinea, Oman) are strongly affected by excessive human activity with a high risk of oil pollution, including shipping, exploration and development of off-shore oil and gas reserves, construction and operation of underwater pipelines, platforms, terminals, storage facilities, ports, etc. Shipping activities certainly causes serious harm to the marine environment, but in the case of discharge of oil-contaminated waters in the coastal zone. We consider such cases in this chapter. In the open ocean, such discharges usually do not take place. But the listed other sources of pollution have been causing more significant harm lately, which is demonstrated, in particular, by satellite monitoring.

First of all, we discuss sea surface oil pollution of anthropogenic origin. Satellite instrumentation and technique for oil pollution monitoring of the seas, as well as examples of oil pollution in different parts of the World Ocean will be presented in this chapter. Satellite instrumentation and technique for evaluation of water quality (suspended matter, algae, wastewater) in lakes and seas are presented in other chapters of this book.

Pollution of marine surfaces with oil-containing films is the main parameter of water pollution which is under satellite monitoring and attention of researchers during four decades starting from the launch of the SEASAT satellite on 27 June 1978 [4, 28, 31, 51, 56, 61, 70, 72, 73, 76]. Methods and technologies developed by scientists for satellite detection of oil pollution at the sea surface began to be applied in the practical monitoring systems [12, 13, 14, 35, 37, 40, 45–46, 50, 52]. For example, in

the Baltic Sea, HELCOM (Helsinki Commission) monitors and annually publishes summary maps of spatial distribution oil spills, but only those that were detected by aerial surveillance, and this is only a few dozen per year [40]. Much more oil spills are detected using satellite methods, for example, in the CleanSeaNet Project of the European Maritime Safety Agency (EMSA) or in the framework of daily operational satellite monitoring of oil pollution in the Southeastern Baltic Sea related to beginning of oil production at the Lukoil D-6 offshore oil platform in 2004 [11, 35, 45–47]. A significant difference between the EMSA cumulative maps of oil pollution and those produced for the Southeastern Baltic Sea is in the algorithms for automatic detection of oil pollution (derived from radar data only) used in EMSA and expert-based approach based on the integrated analysis of SAR (Synthetic Aperture Radar), IR (infrared), optical satellite imagery, meteorological and oceanographic data, as well as numerical modelling of oil spill drift and transformation (Seatrack Web) used for the Lukoil D-6 offshore oil platform monitoring. Our integrated approach to the oil spill monitoring allows significantly reduce the probability of false alarms which is a typical problem for automatic detection systems [40, 46, 50, 52].

Accurate detection of oil slicks in radar images is still an important issue. Quite a number of natural phenomena hamper reliable identification of oil on the sea surface because they produce similar signatures in radar images, especially at low wind. Such "look-alikes" include organic films, algal bloom, some types of ice and snow, water areas shaded by land features, rain cells, upwelling zones, internal waves, and calm water [50, 52]. According to EMSA, false oil spill alarm rate reaches 60% in the coastal zone. This can be clearly seen on the maps of identified oil pollution, which are formed annually by EMSA and are posted on their website. Figure 4.1 shows such a map for 2018. Red circles correspond to higher detection confidence level (Class A), green—a lower detection confidence level (Class B). As can be seen from the figure, the number of green circles prevails, especially in areas where regular observations from aircraft are not carried out.

Monitoring of oil pollution from space is usually carried out using the synthetic aperture radars (SAR) and advanced synthetic aperture radars (ASAR) installed on different satellites. A correct detection of oil spills requires a number of additional information on wind speed and direction, wave height and direction, water and air temperature, ice cover, algal bloom, structure and dynamics of surface mesoscale and sub-mesoscale currents and phenomena, atmospheric fronts to describe the manifestation, transformation and distribution of oil films [46, 50, 52]. Long-term monitoring of ecological state and oil pollution around the Lukoil D-6 offshore oil platform in the Southeastern Baltic Sea has shown that real-time numerical modelling of oil spill drift and transformation is of vital importance for such kind of monitoring systems in any part of the World Ocean [1, 16–20, 23, 33, 69, 81]. In case of the Lukoil D-6 monitoring we successfully used the Seatrack Web model of the Swedish Meteorological and Hydrological Institute (SMHI), which today has a spatial resolution of 2 nautical miles (n m) and a time step of 15 min [6, 36]. Seventeen-year long satellite monitoring of the Southeastern Baltic Sea has shown that mesoscale and sub-mesoscale vortical structures and water dynamics play a crucial role in the transport of the pollutants, thus even much more high spatial resolution is required in

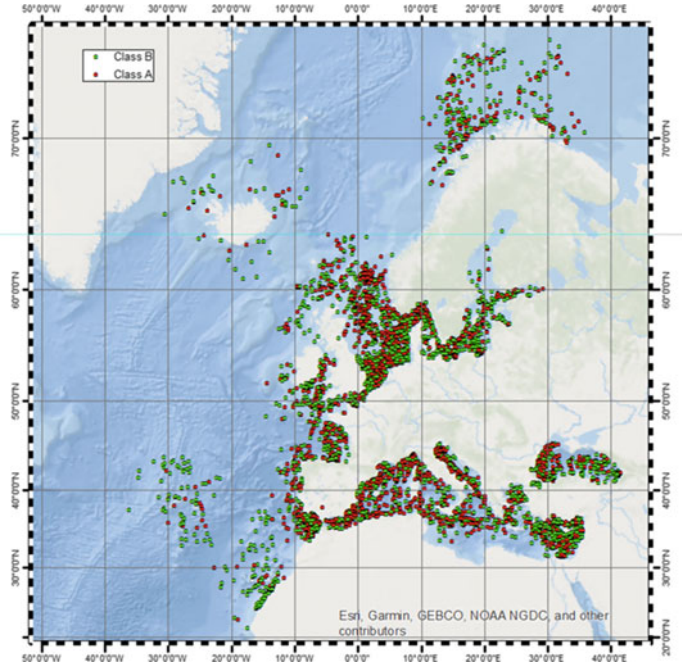


**Fig. 4.1** CleanSeaNet oil spill detection statistics for 2018: dots on the map represent the spills in the European seas which have a higher detection confidence level (in red) and a lower detection confidence level (in green) (http://www.emsa.europa.eu/csn-menu/csn-service.html)

numerical models. Recently, an ultra-high resolution circulation model (0.125 n m grid) of the Southeastern Baltic Sea was compiled from the General Estuarine Transport Model (GETM) in order to simulate the mesoscale and sub-mesoscale eddy field in the area. The model results showed almost the digital twins of eddies revealed with daily optical and infrared satellite imagery available for the period of May–August 2015 [80]. Such kind of ultra-high resolution circulation models could significantly improve a forecast of the oil spill drift.

## 4.2 Physical Principles and Methods of Oil Spill Detection

Currently, radar (SAR) sounding in the microwave range is one of the main methods of remote study of both oceanic processes and processes of interaction between the ocean and the atmosphere. During the past four decades it showed effectiveness in oil spill detection on the sea surface. Radar survey technique is unique in that it obtains high resolution (up to several meters) images in a wide swath, day and night in any season and under any weather/cloud conditions. Active remote sensing of the ocean

surface is based on measuring variation of scattered radar signal. In case of a satellite-based synthetic aperture (SAR) or side-looking radar on the airplane the information about the parameters of the underlying surface is contained in the reflection function, which is observed in the form of an electromagnetic wave backscattered from the sea surface. The reflection function is determined both by the properties of the surface itself, and by the conditions of its formation, i.e., by the system emitted and received signals. The radar image of the sea surface depends on sensing electromagnetic range, polarization and angle of incidence of the radar signal [26, 50].

A radar emits an electromagnetic wave with a length $\lambda$, frequency $f = C/\lambda$, where C is speed of propagation of electromagnetic waves in the medium (in vacuum $3 \cdot 10^8$ m/s), the wave vector indicates the direction of propagation of the wave, as well as the polarization (horizontal or vertical) of the wave. The last property is very important, since the orientation the polarization plane relative to the reflecting surface depends on the wave reflection coefficient. The radar systems are designed to operate in horizontal (H) and vertical (V) planes. As a transmitted signal depolarizes when reaching the Earth surface, a specific SAR can operate in four different polarization combinations: HH, HV, VH, and VV. The first letter refers to the transmitted signal while the second letter refers to the backscattered signal. HH and VV signals are known as co-polarized signals, while HV and VH signals are known as cross-polarized signals [71].

Vertical polarization is used to study a wide class of processes and phenomena that manifest on the sea surface by modulating the gravitational-capillary component of the surface wave spectrum. Horizontal polarization, being less sensitive to variations in the small-scale roughness of the sea surface, is widely used for observing sea ice, and separating areas with ice cover from open water. Since the intensity of scattering by the sea surface is significantly reduced when using radiation and reception at cross polarizations (VH and HV), such modes are used to highlight objects on the sea surface that cause multiple scattering, such as ships and ice cover deformations (hummocks, cracks, cracked ice) [50].

Satellite radars of the first generation had the ability to monitor the Earth on one fixed polarization of the probing signal, the horizontal (HH), for example, the SAR on the Almaz-1, RADARSAT-1, Seasat, JERS-1 satellites, or the vertical (VV)—the SAR on ERS 1/2 satellites. The new generation of satellite radars installed on Envisat, RADARSAT-2 and TerraSAR-X have the ability to survey in various modes: VV, HH, VV/HH, VV/VH, HH/HV [50].

The spectral bands of SAR systems are specified by the following codes: K (0.8–2.5 cm); X (2.5–3.8 cm); C (3.8–7.5 cm); S (7.5–15 cm); L (15–60 cm); and P (60–120 cm). The SARs with wavelengths from 1.11 cm ($f = 27$ GHz) up to 30 cm ($f = 1$ GHz) are used for the ocean studies. Usually radars operate in a pulse mode, although continuous radiation is sometimes used.

The general principle for oil spills detection on the sea surface is known since ancient times when sailors used olive oil or other oily substances to spill over the sea surface to reduce waves around ships. We don't know how really effective was this method during storm conditions, but this physical mechanism works well in damping the gravity-capillary waves (with a characteristic wavelength of several centimeters)

which are always present on the sea surface. Different types of oil products can damp the gravity-capillary waves 10–30 times, and radars working on the same wavelength can easily discriminate water areas with developed from damped gravity-capillary waves. On SAR images water areas with damped gravity-capillary waves look like black zones because the emitted radar signal does not return back to the antenna. Grey areas on SAR images show zones from which the scattered (by gravity-capillary waves) radar signal partially returns back to the radar [3, 7, 21, 25, 31, 58, 74, 79]. Discharges which contain any kind of oil products will result in a formation of an oil slick. This is proved by numerous in-situ measurements done by the Baltic Sea countries and regularly published by HELCOM (https://helcom.fi/wp-content/uploads/2020/01/HELCOM-Aerial-Surveillance-Report-20XX.pdf), as well as by measurements in the North Sea [12], Mediterranean Sea [13, 14], and other regions of the World Ocean. Discharges which does not contain oil products will not result in slicks on the sea surface detected by SAR with the exception of, for example, palm or vegetable oils, but these are very rare cases, especially in large quantities.

There are two obstacles in correct detection of oil spills at the sea surface by this method. The first one is related to the fact that the damping of gravity-capillary waves works well at winds of about 3–8 m/s [50], because light winds do not generate capillary waves, and the sea surface is quasi-calm and smooth enough to reflect the radar signal without scattering back to the radar. This is the reason why calm water looks like an oil spill on the sea surface, as well as a real oil spill can be hidden when released on calm water. Wind force over about 8 m/s leads to wind-wave breaking, mixing in the upper layer, and formation of foam. All this destroys gravity-capillary waves on the sea surface and even an oil spill cannot smooth the sea surface enough to be detected by the radar. Thus, in stormy conditions the whole water area has a grey color where all peculiarities at the sea surface are hidden. The second issue is related to the natural look-alikes in the ocean and atmosphere mentioned above, which can also damp gravity-capillary waves and smooth the sea surface. Thus, radar will not be able to discriminate between an oil spill and a look-alike. Both issues are serious obstacles for a progress in automatic detection of oil spills in SAR images [4, 10, 22, 24, 27, 77]. To overcome this problem we use an expert-based approach which includes integrated analysis of SAR, as well as all available satellite, meteorological and oceanographic data for the area under investigation [46, 50]. Our long-standing experience shows that this integrated approach can significantly reduce the level of false alarms.

## 4.3 Satellites and Sensors

Different SAR systems have been installed on the following satellites [2, 29, 50, 52, 71]: the USA SEASAT with the first spaceborne SAR (27 June–10 October 1978), the USSR Kosmos-1980 (1988) and Almaz-1 (1991–1992), the ESA ERS-1 (1991–2000), the Japanese JERS-1 (1992–2008), the ESA ERS-2 (1995–2011), the Canadian Radarsat-1 (1995–2013), the ESA Envisat (2002–2012), the Japanese ALOS

(2006–2011), the Canadian Radarsat-2 (2007–present), the German TerraSAR-X (2007–present), the Italian COSMO SkyMed (2007–present), the Indian RISAT-2 (2009–present), the German TanDEM-X (2010–present), the Indian RISAT-1 (2012–2017), the Chinese Huanjing-1C (2012–present), the ESA Sentinel-1A (2014–present), the Japanese ALOS-2 (2014–present), the ESA Sentinel-1B (2016–present), the Argentina SAOCOM (2018–present), and the Canadian Radarsat Constellation Mission with three identical spacecrafts (2019–present). Sentinel-1A and Sentinel-1B SAR data are the only ones that are freely available on the internet. SAR imagery can be downloaded from the ESA Copernicus Open Access Hub platform (https://www.sentinel-hub.com/). Spatial resolution of the modern SAR systems installed on the satellites is of 1–5 m [71]. Table 4.1 shows the main characteristics of SAR systems installed on different satellites.

For a brief example let us take the ASAR that was once mounted on the Envisat satellite and widely used for oil pollution monitoring in oceans and seas. It had a phased array antenna with an incidence angle from 15° to 45° and operated in C-band (5.7 cm) in five polarization modes (VV, HH, VV/HH, HV/HH, VH/VV). The obtained data were used in many applications beside oil spill monitoring, such as determining ice cover and ship location and studying some oceanic (currents, fronts, eddies, internal waves) and atmospheric (internal gravity waves, convection, atmospheric fronts and vortices) phenomena and processes. The ASAR design allowed adapting the survey configuration (polarization, resolution, swath width) to the specifics of the object of observation.

The ASAR Wide Swath Mode (WSM) surveying provided the ability to survey in a 400 km swath with a spatial resolution of 150 m $\times$ 150 m at one of the selected polarizations of the signal (VV or HH) and allowed obtaining radar images of the same area with a period of repeated observations from 1 day in the polar regions to 1 week at the Equator. Alternating Polarization Mode (APM) allowed receiving simultaneous image pairs of the underlying surface formed at different combinations of polarizations of the radiated and received radar signals, namely VV/HH, HH/HV and VV/VH in a 100 km wide swath and with a spatial resolution of up to 30 m. When working in a narrow swath (Image Mode), the phased antenna array by changing the angle of radiation of the signal allowed to select any of 7 bands and obtain an image with a high spatial resolution (30 m $\times$ 30 m) at one of the selected polarizations VV or HH ranging in size from 56 km (7th band) to 100 km (1st band). Envisat completed its work in orbit on April 8, 2012. Since 2014, Sentinel $-1$A/$-1$B data, which is freely available from ESA, have become the most widespread.

## 4.4 Examples of Oil Spill Pollution

In this Section we present examples of oil pollution of the ocean surface acquired by different satellites. From April 20 to May 28, 2010 we daily followed the evolution of oil pollution in the Gulf of Mexico which resulted from the accident on the *BP Deepwater Horizon* oil platform that occurred on April 20, 2010 [49, 50]. The

**Table 4.1** The main characteristics of SAR systems on satellites (based on data presented in [29, 50, 52, 71]

| | SEASAT | ERS-1/2 | Almaz-1 | JERS-1 | Radarsat-1 | Envisat | Radarsat-2 | Terra-SAR-X | Sentinel-1 A/B |
|---|---|---|---|---|---|---|---|---|---|
| Country/agency | USA | ESA | USSR | Japan | Canada | ESA | Canada | Germany | ESA |
| Year of launch | 1978 | 1991/1995 | 1991 | 1992 | 1995 | 2002 | 2007 | 2008 | 2014/2016 |
| Range | L | C | S | L | C | C | C | X | C |
| Frequency, GHz | 1.275 | 5.25 | 3.1 | 1.275 | 5.3 | 5.7 | 5.3 | 9.65 | 5.405 |
| Wavelenght, cm | 23.5 | 5.66 | 9.6 | 23.5 | 5.66 | 5.66 | 5.66 | 3.13 | 5.55 |
| Polarization | HH | VV | HH | HH | HH | HH, VV, VH, HV | HH, VV, VH, HV | HH, VV, VH, HV | HH/HV, VV/VH |
| Incidence angle, ° | 20 | 23 | 17–62 | 39 | 20–50 | 15–45 | 20–60 | 20–55 | 18.3–47 |
| Swath width, km | 100 | 100 | 30–60 | 75 | 50–500 | 56–400 | 18–500 | 10/30/100 | 80/250/400 |
| Spatial resolution, m | 25 | 25 | 25 | 18 | 8–100 | 25–150 | 3–100 | 1/3/16 | 3.5–40 |

development of the situation was traced on the basis of a joint analysis of optical (MODIS-Aqua, MODIS-Terra) and radar images (ASAR Envisat), which proved to be very effective since the optical images made it possible to exclude from consideration the areas of calm water on the ASAR images (Fig. 4.2). Also, the radar images gave more complete information about dimensions of the areas covered with oil films indiscernible on optical images. The uniqueness of this accident was in a very large oil spill (up to 23,000 $km^2$) which was continuously fed during several months by

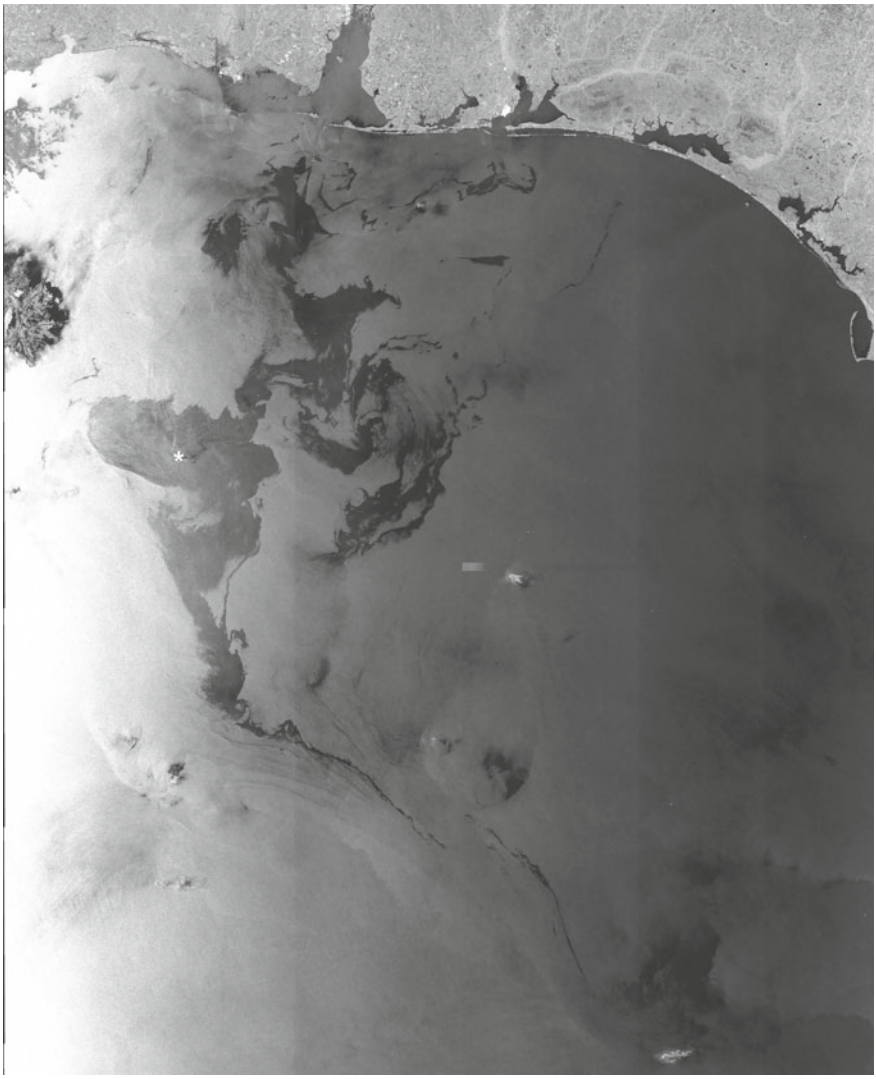

**Fig. 4.2** Oil spills (black patches) in the northern part of the Gulf of Mexico on the ASAR Envisat image obtained on June 3, 2010 (03:44 UTC). The accident area is asterisked. (© ESA, 2010)

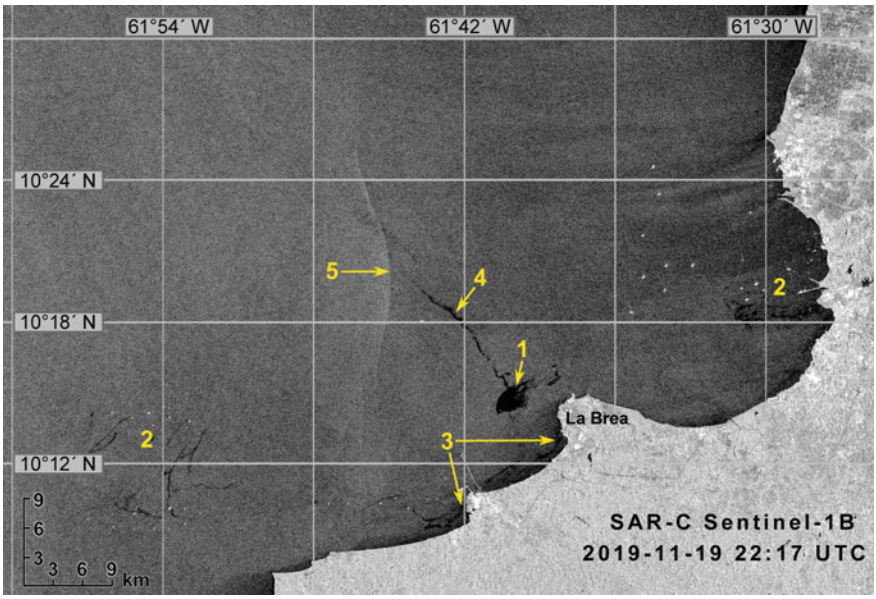


**Fig. 4.3** Oil spills off Point Fortin, southwestern Trinidad, the Caribbean (SAR C Sentinel-1B, 19 November 2019, 22:17 UTC). See text for explanation of numbers

oil flux from a well with a discharge of about 800 ton per day at a depth of 1500 m on the seafloor [49]. This ecological catastrophe was one of the largest in the US history.

Figure 4.3 shows western coast of Trinidad and Tobago, the Caribbean on 19 November 2019. Several oil spills were observed in the coastal zone off Point Fortin: (1) oil spill from the anchored ship, oil spill area is of 3.5 $km^2$; (2) oil pollution at anchorage of ships; (3) wastewater discharges from coasts; (4) discharge from a moving vessel, length of oil spill is of 6.5 km; (5) surface manifestation of internal wave train. Point Fortin, officially the Republic Borough of Point Fortin, the smallest Borough in Trinidad and Tobago, is located in southwestern Trinidad. After the discovery of oil reserves in the area in 1906, the town grew into a major oil-producing center with an economic culmination between the 1940s and 1980s. A construction of a liquefied natural gas plant by Atlantic LNG in late 1990s revived the economy. The LNG terminal is located in the Port of Point Fortin.

Another area of regular oil pollution is in the eastern part of the Gulf of Guinea at the confluence of the three branches of the Niger River, as shown by long-term satellite observations (Fig. 4.4). The largest area of marine surface pollution was caused by an accidental discharge. On 20 December 2011, the Shell's Bonga offshore oil spill of 40,000 barrels resulted from the routine transfer of crude oil from the *Bonga* floating production, storage and offloading vessel (FPSO) to a waiting oil tanker in the Gulf of Guinea [44]. An export line linking the FPSO and the tanker was identified as the likely source of leakage. It was likely the largest oil spill which

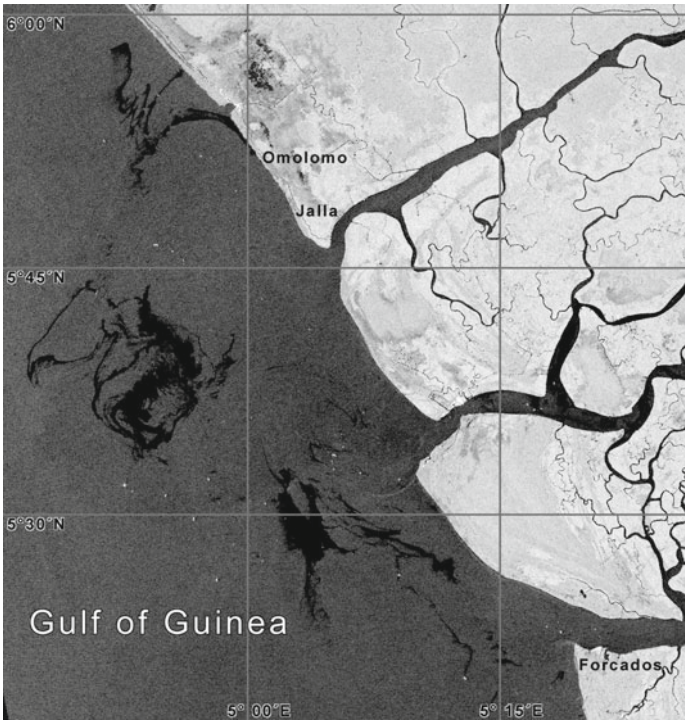


**Fig. 4.4** Oil pollution in the Gulf of Guinea. (SAR C Sentinel-1A, 08 February 2022, 17:53 UTC) (©ESA 2022). Ships in the sea are visible as bright white dots

had occurred offshore Nigeria since 1998. The spill was clearly detected on the ASAR Envisat image acquired on 21 December 2011, 09:30 UTC, as well as quite well visible on the MODIS-Terra optical image. At the acquisition time, the spill was 80 km long, 15 km wide, and had a total area of 923 km$^2$. Beside this huge oil spill in the region of the *Bonga* FPSO vessel, a number of other cases of oil pollution of coastal waters were identified in the same ASAR image of 21 December 2011 [44]. The total area of 11 large spills, excluding the Bonga one, was over 100 km$^2$. Moreover, three river plumes from the Niger River arms polluted with oil products were also detected with a total area of 78 km$^2$ [44]. Terleeva et al. [75], based on the analysis of ASAR Envisat medium resolution imagery taken off western coast of Central Africa for 2003–2009, showed that the largest number of oil spills was observed along the coast of Nigeria (148), Cameroon and Equatorial Guinea (98), Ghana (49), Cote d'Ivoire (31), and Togo/Benin (9). Individual oil spill area varied from 0.5 to 80 km$^2$. These case studies, based on irregular satellite information, confirm that coastal waters of Nigeria are highly polluted.

Figure 4.5 shows numerous ships visible as bright white dots and oil spills in the Hormuz Strait, the Persian Gulf, in front of Port of Bandar Abbas on 4 April 2020. Bandar Abbas is a port city and capital of Hormozgān Province on the southern coast

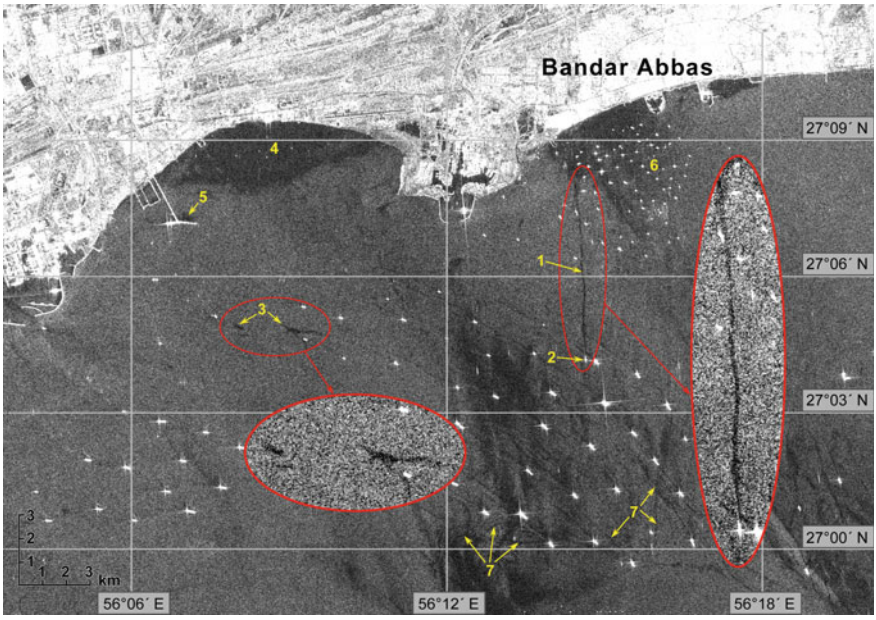


**Fig. 4.5** Oil spills off Bandar Abbas in the Hormuz Strait, the Persian Gulf (SAR C Sentinel-1A, 4 April 2020, 14:17 UTC). See text for explanation of numbers

of Iran on the Persian Gulf. The port occupies a strategic position in the narrow Strait of Hormuz, and it is the location of the main Iranian Navy base. A significant part of the trade between Iran and other countries of the world is carried out through this port. Numbers on the Fig. 4.5 show: (1) discharge from a moving vessel, length of oil spill is of 5 km; (2) ship from which polluted water was discharged; (3) oil spill from the anchored ship; (4) near-shore area of turbid water; (5) wastewater discharges from a pier; (6) ships; (7) accumulation of films of surface-active substances (biogenic films) in convergent zones of currents.

Sentinel-1A and Sentinel-1B SAR imagery for 2018 and 2019 clearly reveal cases of oil pollution in the Port of Suez (Gulf of Suez, the northern part of the Red Sea) (Fig. 4.6), as well in the areas of major tourist resorts of Egypt on the Red Sea [34]. We found that the dirtiest area in the Northern Red Sea is the Port of Suez area where ships are waiting for the passage through the Suez Canal. A series of SAR images for different dates of 2018–2019 showed that almost in every satellite image there is one or several oil spills, as well as films of surface active substances (oily and waste waters). The coastal zones around Hurghada and Sharm el-Sheikh resorts looks quite clean, but even here small-size oil spills occur as well [34]. Egypt seems to be at risks of oil pollution impacts because it has a series of largest tourist resorts streched for dozens of km along the coast, and the extensive shipping traffic which goes to the Gulf of Suez and further via the Suez Canal to the Mediterranean Sea, as well as

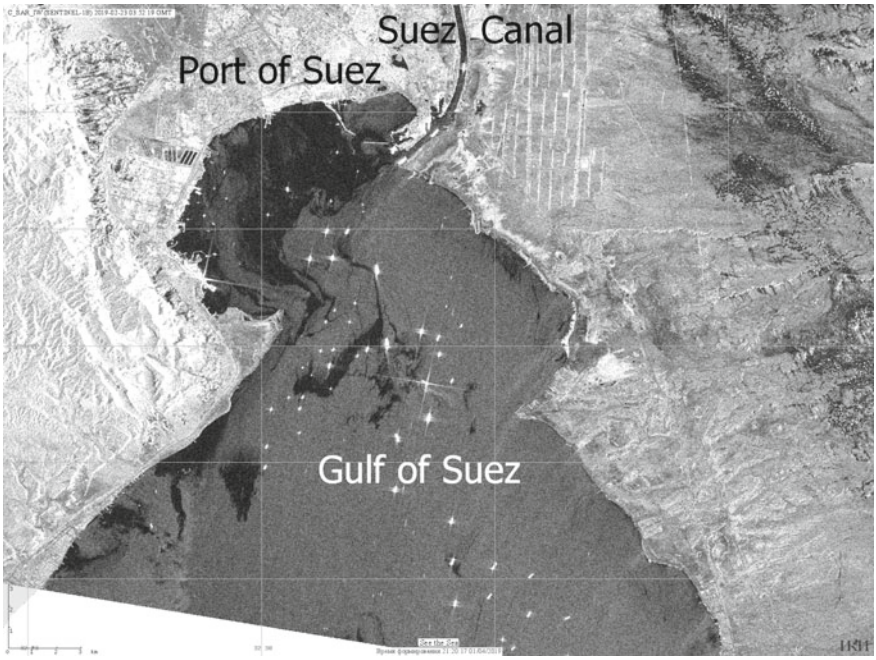


**Fig. 4.6** SAR-C Sentinel-1B image of Port Suez in the Gulf of Suez on 23 February 2019, 03:52:19 GMT. Black patches are oil spills and white dots are ships

to the Gulf of Aqaba. This ship traffic carries about 15% of all global maritime trade and 10% of global seaborne oil passing through the Red Sea and the Suez Canal.

It is evident that the above mentioned ship traffic should have the same oil pollution effect on the other side of the Suez Canal in the Southeastern Mediterranean Sea. About 17,550 ships passed through the Suez Canal in 2017. Beside the very busy ship traffic in the Mediterranean waters of Egypt, in the last decade, there has been a substantial development of offshore gas and oil fields along the Mediterranean coasts of Egypt, where the most active companies are BP, BG, Eni, IEOC, EGAS, Total, RWE Dea and Dana Gas [39]. Indeed, our preliminary research for oil pollution in coastal waters of Egypt based on the analysis of the Sentinel-1A and Sentinel-1B SAR imagery for 2017–2019 showed large concentration of oil spills in the offshore area between Damietta and Port Said, which coincides both with maritime traffic related to the Suez Canal and offshore activities related to gas exploration and production (Fig. 4.7). Two dozen SAR images showed that almost in every satellite image there is one or several oil spills, as well as films of surface-active substances (oily and waste waters) in the coastal waters of Egypt [39].

The port of Kaliningrad is situated on the southeastern coast of the Baltic Sea. The only Russia's ice-free port on the sea, it comprises a commercial sea port, a river port, a sea fishing port and Kaliningrad Sea Canal. Container lines connect to the Netherlands, UK, Germany, Poland and Lithuania. In 2010–2020, Kaliningrad port

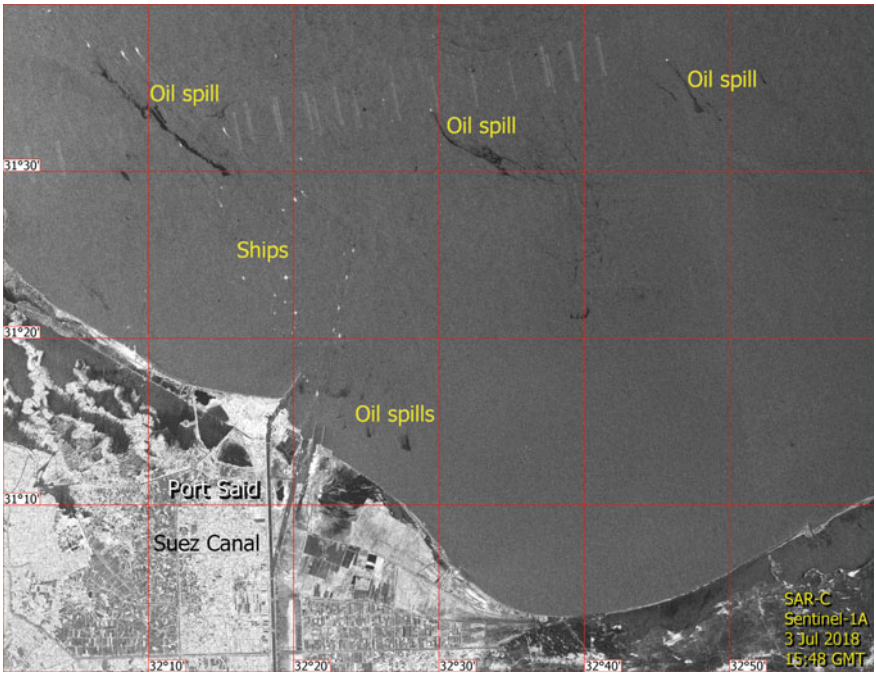


**Fig. 4.7** SAR-C Sentinel-1A image of oil pollution offshore of Port Said, the Southeastern Mediterranean Sea on 3 July 2018, 15:48 GMT. Black patches are oil spills and white dots are ships and offshore platforms

turnover ranged 2–4 million tons. Vessels are awaiting pilotage to the port anchor at the entrance to Kaliningrad Sea Canal, near the town of Baltiysk. In the Russian Baltic, the risk of oil pollution is mostly associated with tanker and ship traffic to and from the port of Kaliningrad.

In 2004, a complex environmental monitoring project was launched by LUKOIL-Kaliningradmorneft in connection to offshore oil production at Kravtsovskoye (D-6) field. The platform is mounted on the sea bottom at a depth of 30 m, at a distance of 22.5 km from the Curonian Spit and 8 km from the Lithuanian sea border. The monitoring routine included satellite remote sensing of oil pollution in the vicinity of the platform and in a larger adjacent area of about 60,000 km$^2$ in the south-eastern Baltic, i.e. nearly 1/6 of the total Baltic Sea area. Operational receiving, processing and analysis of various data from ENVISAT ASAR, RADARSAT SAR, NOAA AVHRR, Terra/Aqua MODIS, TOPEX/Poseidon, and Jason-1 instruments was organized on a daily basis in order to accurately detect oil spills and effectively reduce false alarms from look-alikes [11, 35, 43, 45–48]. It is noteworthy that this near-real time monitoring system, that we organized in 2004, was the first one in Russia and up to date remains the only such system still in operation.

Since 2003, satellite monitoring of oil pollution in the Baltic, Black and Caspian Seas has been regularly performed by Space Research Institute of Russian Academy

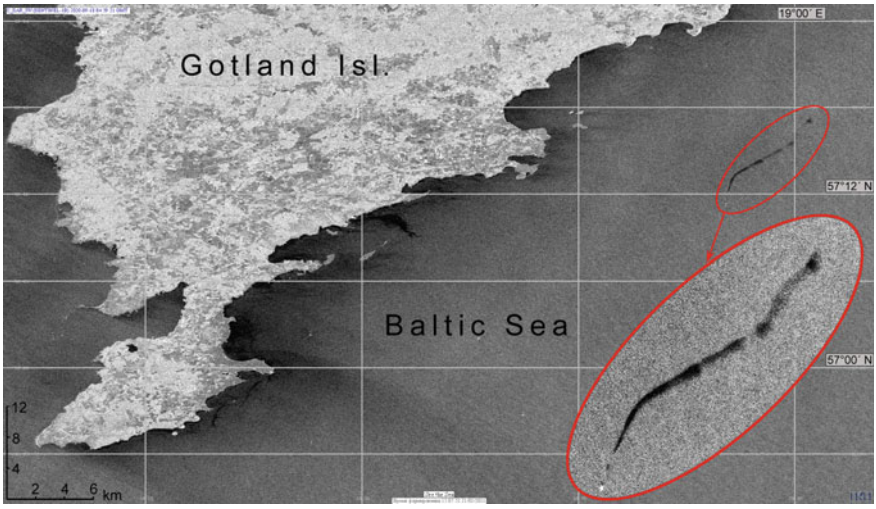


**Fig. 4.8** Oil spill detected near Gotland Island in the Baltic Sea on SAR-C Sentinel-1B, 18 September 2020, 04:59 UTC

of Sciences in the framework of national and international research projects. This unique monitoring with an analysis of several thousands of SAR images gave detailed statistical information on the spatial and temporal distribution of oil spills as well as individual characteristics of oil spills detected.

For example the monitoring of the Southeastern part of the Baltic Sea [44, 52] showed that the individual oil spill area varied from 0.1 to 105 $km^2$, and yearly total surface of oil pollution varied from 150 to 830 $km^2$ [11, 47]. The largest number of oil spills is regularly found along the main shipping routes. Figure 4.8 shows one of the recent examples of oil spills detected along the shipping route east of Gotland Island. Length of oil spill is of 11.5 km.

Satellite monitoring for the Black Sea showed that similar to the Baltic, North and Mediterranean seas, the detected oil spills are accumulated along the main shipping routes coming to the main ports and sea terminals. For the Black Sea, these are routes from the Bosphorus Strait to Odessa (Ukraine), Kerch Strait between the Black Sea and the Sea of Azov, Novorossiysk (Russia), and ports of Georgia [8, 9, 50, 52, 59, 62, 72]. Figure 4.9 shows one of the recent examples of oil spills detected in the Black Sea. Numbers 1 and 2 indicate discharges of water containing oil products from standing ships. The area of spot 1 was 1.5 $km^2$, and spot 2 was 1.6 $km^2$. The length of oil slick 3 caused by a discharge from a moving vessel was 21.4 km.

Satellite monitoring of oil pollution in the Caspian Sea [50, 52, 53, 60, 63, 64] allowed to show that the most polluted area of the Caspian Sea is located around Neftyanye Kamni (Oily Rocks), one of the oldest oil production area located eastward of Absheron Peninsula, Azerbaijan [52, 64]. Figure 4.10 shows one of the recent examples of oil spills detected around Neftyanye Kamni and other offshore

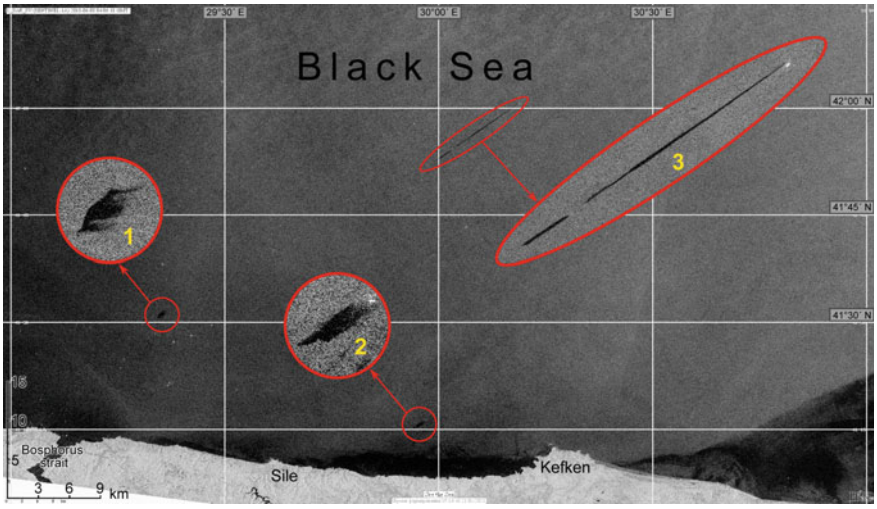


**Fig. 4.9** Oil spills detected in the Black Sea eastward of the Bosphorus Strait on SAR-C Sentinel-1A, 08 June 2018, 04:06 UTC. See text for explanation of numbers

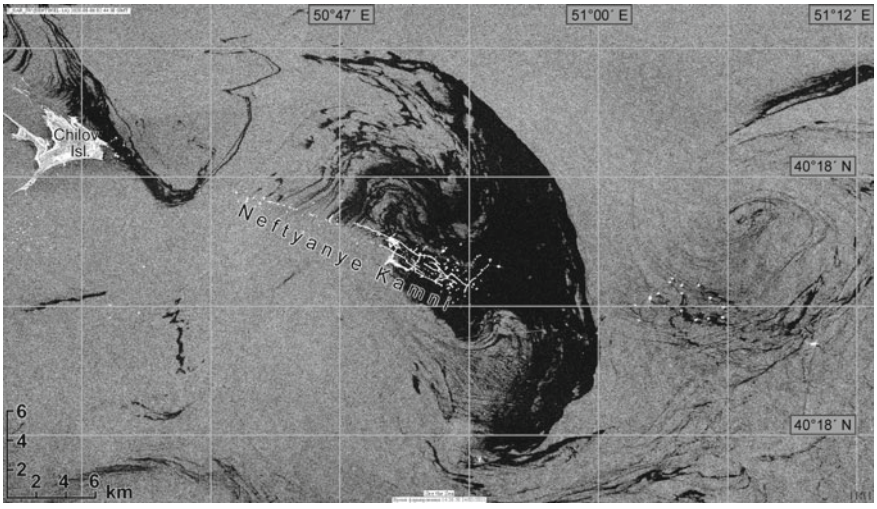


**Fig. 4.10** Oil spill detected around Neftyanye Kamni in the Caspian Sea on SAR-C Sentinel-1A, 06 August 2020, 02:44 UTC

oil platforms in the Caspian Sea. The area of oil spill around Neftyanye Kamni is 251 km$^2$.

Discharges from ships in the Caspian Sea are identified in SAR images much less frequently than oil pollution around offshore oil platforms or petroleum hydrocarbons emission from the seabed [64], and they are usually observed along shipping routes.

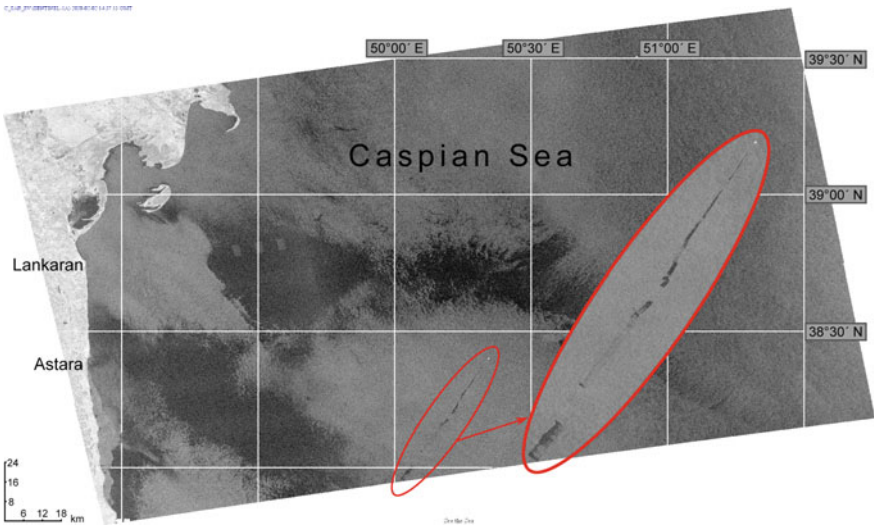


**Fig. 4.11** Oil spill detected in the south-eastern part of the Caspian Sea on SAR-C Sentinel-1A, 02 February 2020, 14:37 UTC

Figure 4.11 shows just such a case. The length of the oil slick caused by a discharge from a moving vessel is 56 km.

## 4.5 Discussion

Forty-year-long history of SAR application in satellite monitoring of oil pollution has proved the efficiency of this kind of instruments and methods for reliable detection of oil spills on the sea surface. Of course, there are some weather restrictions for use of SAR systems as well as natural look-alikes caused by different ocean and atmosphere features and processes, but they do not outweigh the benefits of this remote sensing method. We can list the following advantages of SAR systems in oil spill detection:

1. Round-the-clock work due to the use of active sensing, and the image characteristics do not depend on the time of the day and solar illumination (night, Polar night);
2. Imaging is almost independent of the weather because microwave radiation freely penetrates the atmosphere and clouds;
3. The uniformity of water microwave dielectric properties implies that backscatter variations originate only from the geometry of the disturbances, which makes satellite data interpretation far less complicated;;
4. High spatial resolution (several meters) in a wide swath (300–400 km);
5. Regular monitoring (up to daily, and even several times per day) of any water areas of the World Ocean remotely;

6. Possibility to organize near-real-time monitoring, a SAR image can be received 30–60 min after a satellite passage over the monitoring area;
7. Low cost of satellite monitoring in comparison with aerial surveillance and ship patrolling.

Concerning the drawbacks of this method, we can list the following issues:

1. Presence of look-alikes on the sea surface (see Table 4.2).
2. Restrictions related to wind speed of 3–8 m/s, when this method works well. Big problems in identification of oil spills arise in calm water and storm conditions.
3. Difficulties in oil spill detection in presence of sea ice.
4. Relatively high cost of one SAR image, which is a problem for scientific research, which sometimes requires hundreds of images. The cost of SAR

**Table 4.2** The main types of the oil spill "look-alikes" and their radar manifestations on the sea surface

| Hydrophysical process | The shape of the manifestation on the radar image | Areas of origins | Hydrometeorological conditions |
|---|---|---|---|
| Biogenic surface films | Display the structure of surface currents | Coastal zones | Destroyed when wind speed >7 m/s |
| Local wind weakening areas | Extensive areas of reduced backscattering | Everywhere | Wind speed <2 m/s |
| Areas of wind shadows | Areas of reduced backscattering oriented along the wind direction | In the vicinity of the mountainous terrain shoreline | Even with strong winds up to 15 m/s |
| Rain cells | Light-colored cellular structures with a dark center | Everywhere | Intense rains and strong winds |
| Boundary of the hydrological or atmospheric front | Wide dark band with irregular edges, which are caused by unsteadiness of the frontal zone | Everywhere | Presence of a hydrological or atmospheric front |
| Ocean internal waves | Thin quasi-periodic bands of radar signal amplification and attenuation | Continental slope | Wind speed <8 m/s |
| Atmospheric internal gravity waves | Wide quasi-periodic bands of radar signal amplification and attenuation | Everywhere | Stable stratification of the near-water atmospheric layer, shear currents in atmosphere |
| Young ice | Extensive areas of reduced radar scattering | Usually near shoreline, at the edge of the ice sheet | Cold season |
| Areas with algal bloom | Low backscatter levels | Everywhere | Warm season |

imagery significantly increases in the direction of the near- and real-time monitoring, when satellite data are delivered in one or several hours. Sentinel-1A and Sentinel-1B SAR data are the only ones that are freely available on the internet now, but with a delay of about a day.

Automatic identification of oil pollution leads to a large false alarm in the case of oil look-alike on the sea surface. It is especially difficult to distinguish between anthropogenic and biogenic films. For confident detection of exactly oil pollutions an expert analysis is required. The expert takes into account all local peculiarities, hydrometeorological factors like wind speed, atmospheric fronts, rain, ice cover, upwelling, water dynamics, as well as algal bloom, and previous SAR images. When possible, satellite optical data are used as additional information on the sea surface.

We have to note also, that oil pollution monitoring in the Mediterranean, North, Baltic Seas, as well as in USA and Canada is normally carried out by special patrol aircrafts and ships. Different countries have different number of patrol aircrafts which are equipped by different sets of the monitoring instruments from simple visual observations to a complete set of the following sophisticated sensors, which should be regarded as remote sensing instruments as well [5, 30]:

- Side-Looking Airborne Radar (SLAR);
- Infrared/Ultraviolet (IR/UV) sensor which is a passive sensor using reflected sunlight in the ultraviolet region (0.32–0.38 micron) for detecting oil spills;
- Microwave radiometer (MWR) which is a passive sensor and is used for oil spill detection and oil thickness measurements. Oil emits stronger microwave radiation than water and appears brighter than the water (which is dark in the background);
- Laser FluoroSensors (LFS) and Scanning Laser Environmental Airborne Fluorosensor (SLEAF) sensors were found to be the best available sensors for oil spill detection since they both detect and classify oil on all surfaces and also operate in the day or night conditions;
- Forward-Looking IfraRed (FLIR) camera provides longwave infrared imaging for oil spill detection in field conditions;
- Laser-Ultrasonic Remote Sensing of Oil Thickness (LURSOT) sensor which detects the oil based on its acoustic or mechanical properties rather than its optical and electromagnetic properties. Absolute oil thickness can be measured using this technique. The laser-acoustic sensor is an active sensor and can operate day and night;
- Video camera for recording visual observations of oil pollution.

Aerial surveillance has its own advantages and disadvantages in comparison with satellite remote sensing. The surveys are expensive and depend on the availability of multiple instruments, weather conditions and time of the day. As a rule, they are conducted in daylight in good weather. Very often sea areas under monitoring are located far from the base airports for patrol aircrafts, and it takes time to go to the oil spill location and back. Usually, aircrafts cannot perform transboundary monitoring flights over water area of the neighboring country. Aerial survey theoretically requires

about 10 flight hours to monitor the area of 300 km × 300 km which is a typical frame for one Radarsat SAR image taken instantly.

To rise the efficiency of the aerial surveillance authorities have to improve the tactics of aerial observations, which has to take into account the real traffic along the main ship routes, operational information from the AIS and port authorities, to increase the number of night flights, and probably to use unmanned aerial vehicles (UAV), which have now a wide range of research and civilian applications, as well as more than 12 h endurance and range more than 200 km [41].

Satellite remote sensing of oil pollution allows to build accumulative maps of oil spills detected in different seas during years (see Fig. 4.1 as an example). These maps can be found in the following publications: for the Baltic Sea [11, 47, 48], the Mediterranean Sea [13, 14], the Black Sea [52] and the Caspian Sea [52, 63]. Having such a huge statistics on oil spills and general information on oil pollution it is interesting to get an answer to the question—what is the level of oil pollution of the World Ocean and inland seas?

Kostianoy and Lavrova [42] and Carpenter and Kostianoy [15] summarized the following information on the oil pollution in different seas:

1. Total yearly oil pollution of the World Ocean from all sources is estimated at 1.7 to 8.8 million tons (the more realistic value was about 3.2 million tons) in 1970s [32, 65], 0.47–8.3 (1.3) million tons in 1990s [68], and 2.6–4.8 million tons in 2000s [57], which is about 0.05–0.1% from the world oil production (4.76 billion tons in 2011).
2. Oil pollution of the Baltic Sea is estimated at 20–60,000 tons per year. The realistic value seems to be between 1000 and 5000 tons [42].
3. Oil pollution of the North Sea is estimated at 15,000–60,000 tons per year plus the authorized dumping of 10,000–20,000 tons [66, 67].
4. In the Mediterranean Sea it has been estimated at 1600–1,000,000 tons per year. The realistic value seems to be between 50,000 and 100,000 tons per year [15, 38, 78].

## 4.6 Conclusions

In summary, we have to admit that the real amount of oil pollution in the World Ocean and inland seas is still unknown. According to various sources, both the number of observed spills and total volume of spilt oil differ dramatically, sometimes a thousand times. An obvious explanation lies with the differences in the observation techniques, i.e. aerial surveillance, satellite monitoring, and in-situ measurements with varying instruments. Oil spill statistics obtained by different techniques are incomplete and incomparable even within one sea. There is a variety of factors that matter: the number of patrol ships, aircrafts and helicopters per country and per unit of the sea area; the number of flight hours per country and per unit of the sea area; the number of night flight hours; availability of different sensors on the aircrafts; usage of the satellites, etc.

As long-term experience shows, the satellite-based synthetic aperture radar remains the principal instrument for oil pollution monitoring. In spite of the known disadvantages mentioned above (dependence on wind speed, oil look-likes, etc.), it allows receiving high spatial resolution data on an operational basis. In order to reduce the percentage of false alarms, it is reasonable to use an integrated approach to monitoring that combines multisensor and multiplatform satellite survey with analysis of metocean data and local water area features with the help of qualified and experienced operators. For operational monitoring of large water areas, e.g. the entire Mediterranean Sea, it is necessary to develop methods of automatic detection of oil pollution.

**Acknowledgements** The research was partially funded in the framework of the Russian Science Foundation no. 19-77-20060 Project «Assessing ecological variability of the Caspian Sea in the current century using satellite remote sensing data» (2019–2022). This publication was prepared in the framework of the scientific activities related to "The Caspian Sea Digital Twin" Programme performed in the framework of the UN Decade on Ocean Science for Sustainable Development (2021–2030).

## References

1. Ainsworth CH, Chassignet EP, French-McCay D, Beegle-Krause CJ, Berenshtein I, Englehardt J, Fiddaman T, Huang H, Huettel M, Justic D, Kourafalou VH, Liu Y, Mauritzen C, Murawski S, Morey S, Özgökmen T, Paris CB, Ruzicka J, Saul S, Shepherd J, Socolofsky S, Solo Gabriele H, Sutton T, Weisberg RH, Wilson C, Zheng L, Zheng Y (2021) Ten years of modeling the Deepwater Horizon oil spill. Environ Model Softw 142:105070, https://doi.org/10.1016/j.envsoft.2021.105070
2. Alpers W (2014) Remote sensing of African coastal waters using active microwaves instrument. In: Barale V, Gade M (eds) Remote sensing of the African Seas. Springer, Netherlands, pp 75–94
3. Alpers W, Hühnerfuss H (1989) The damping of ocean waves by surface films: a new look at an old problem. J Geophys Res 94:6251–6265
4. Alpers W, Holt B, Zeng K (2017) Oil spill detection by imaging radars: challenges and pitfalls. Rem Sens Environ 201:133–147. https://doi.org/10.1016/j.rse.2017.09.002
5. Al Shammari A (2018) Oil spills detection by means of UAS and inexpensive airborne thermal sensors. Open Access Master's Thesis, Michigan Technological University, p 70. https://doi.org/10.37099/mtu.edu/dc.etdr/607
6. Ambjörn C, Liungman O, Mattsson J, Håkansson B (2014) Seatrack web: the HELCOM tool for oil spill prediction and identification of illegal polluters. In: Kostianoy A, Lavrova O (Eds.) Oil pollution in the Baltic sea. The handbook of environmental chemistry, vol 27. Springer, Berlin, Heidelberg. https://doi.org/10.1007/698_2011_120
7. Bass FG, Puzenko SA (1994) Detection of oil spills on the sea using radar measurements. J Electromagn Waves Appl 8(7):859–870. https://doi.org/10.1163/156939394X00623
8. Bedritskii AI, Asmus VV, Krovotyntsev VA, Lavrova OYu, Ostrovskii AG (2007) Satellite monitoring of pollution in the Russian sector of the Azov and Black Seas in 2003–2007. Russ Meteorol Hydrol 32(11):669–674
9. Bedritskii AI, Asmus VV, Krovotyntsev VA, Lavrova OYu, Ostrovskii AG (2009) Space monitoring of pollution of the Russian sector of the Azov-Black Sea basin in 2008. Russ Meteorol Hydrol 34(3):137–147

10. Brekke C, Solberg A (2005) Oil spill detection by satellite remote sensing. Rem Sens Environ 95:1–13
11. Bulycheva EV, Krek AV, Kostianoy AG, Semenov AV, Joksimovich A (2016) Oil pollution in the Southeastern Baltic Sea by satellite remote sensing data in 2004–2015. Transp Telecommun 17(2):155–163
12. Carpenter A (ed) (2016) Oil pollution in the North Sea. Springer International Publishing AG, Cham, Switzerland, p 312. https://doi.org/10.1007/978-3-319-23901-9
13. Carpenter A, Kostianoy AG (eds) (2018a) Oil pollution in the Mediterranean sea: Part I—the international context. Springer International Publishing AG, Cham, Switzerland, p 350. https://doi.org/10.1007/978-3-030-12236-2
14. Carpenter A, Kostianoy AG (eds) (2018b) Oil pollution in the Mediterranean sea: Part II—national case studies. Springer International Publishing AG, Cham, Switzerland, p 291. https://doi.org/10.1007/978-3-030-11138-0
15. Carpenter A, Kostianoy AG (2018c) Conclusions for Part I: the international context. In: Carpenter A, Kostianoy AG (eds) Oil pollution in the Mediterranean sea: Part I—the international context. Springer International Publishing AG, Cham, Switzerland, pp 325–344
16. Cheng Y, Li X, Xu Q, Garcia-Pineda O, Andersen OB, Pichel WG (2011) SAR observation and model tracking of an oil spill event in coastal waters. Mar Pollut Bull 62(2):350–363. https://doi.org/10.1016/j.marpolbul.2010.10.005
17. Cucco A, Daniel P (2018) Numerical modeling of oil pollution in the Western Mediterranean sea. In: Carpenter A, Kostianoy A (eds) Oil pollution in the Mediterranean sea: Part I. The handbook of environmental chemistry, vol 83. Springer, Cham. https://doi.org/10.1007/698_2016_99
18. De Dominicis M, Pinardi N, Zodiatis G, Archetti R (2013) MEDSLIK-II, a Lagrangian marine surface oil spill model for short-term forecasting—Part 2: numerical simulations and validations. Geosci Model Dev 6:1871–1888. https://doi.org/10.5194/gmd-6-1871-2013
19. De Padova D, Mossa M, Adamo M et al (2017) Synergistic use of an oil drift model and remote sensing observations for oil spill monitoring. Environ Sci Pollut Res 24:5530–5543. https://doi.org/10.1007/s11356-016-8214-8
20. Dietrich JC, Trahan CJ, Howard MT, Fleming JG, Weaver RJ, Tanaka S, Luettich L, Yu RA, Dawson CN, Westerink JJ, Wells G, Lu A, Vega K, Kubach A, Dresback KM, Kolar RL, Kaiser C, Twilley RR (2012) Surface trajectories of oil transport along the Northern Coastline of the Gulf of Mexico. Cont Shelf Res 41:17–47. https://doi.org/10.1016/j.csr.2012.03.015
21. Espedal H, Wahl T (1999) Satellite SAR oil spill detection using wind history information. Int J Rem Sens 20(1):49–65
22. Fiscella B, Giancaspro A, Nirchio F, Pavese P, Trivero P (2000) Oil spill detection using marine SAR images. Int J Rem Sens 21(18):3561–3566. https://doi.org/10.1080/014311600750037589
23. French-McCay DP, Spaulding ML, Crowley D, Mendelsohn D, Fontenault J, Horn M (2021) Validation of oil trajectory and fate modeling of the Deepwater horizon oil spill. Front Mar Sci 8:618463. https://doi.org/10.3389/fmars.2021.618463
24. Gade M (2006) On the imaging of biogenic and anthropogenic surface films on the sea by radar sensors. In: Gade M, Hühnerfuss H, Korenowski GM (eds) Marine surface films: chemical characteristics, influence on air-sea interactions, and remote sensing. Springer, Heidelberg, pp 189–204
25. Gade M, Alpers W (1999) Using ERS-2 SAR images for routine observation of marine pollution in European coastal waters. Sci Total Environ 237–238(441–448):3
26. Gade M, Alpers W, Bao M (1996) Measurements of the radar backscattering over different oceanic surface films during the SIR-C/XSAR campaigns. In: Proceedings of international geoscience and remote sensing symposium (IGARSS'96), vol 2, pp 860–862
27. Holt B, Zeng K (2017) Oil spill detection by imaging radars: challenges and pitfalls. Rem Sens Environ 201:133–147. https://doi.org/10.1016/j.rse.2017.09.002
28. Ivanov AYu (1998) Assessment of marine oil pollution using KOSMOS-1870 and ALMAZ-1 radar images. Mapp Sci Rem Sens 35(3):202–217. https://doi.org/10.1080/07493878.1998.10642092

29. Jackson CR, Apel JR (2004) Synthetic aperture radar marine user's manual. US Department of Commerce, National Oceanic and Atmospheric Administration, Washigton, USA. http://www.sarusersmanual.com. Accessed on 15 February 2021
30. Jha MN, Levy J, Gao Y (2008) Advances in remote sensing for oil spill disaster management: state-of-the-art sensors technology for oil spill surveillance. Sensors 8(1):236–255. https://doi.org/10.3390/s8010236
31. Hovland HA, Johannessen JA, Digranes J (1994) Slick detection in SAR images. In: Proceedings of IGARSS'94, pp 2038–2040
32. Izrael YuA, Tsyban AV (2009) Anthropogenic ecology of the ocean. Nauka, Moscow, p 532 (in Russian)
33. Klemas V (2010) Tracking oil slicks and predicting their trajectories using remote sensors and models: case studies of the Sea Princess and Deepwater Horizon oil spills. J Coastal Res 26(5):789–797. West Palm Beach (Florida), ISSN 0749-0208
34. Kostianaia EA, Kostianoy AG, Lavrova OYu, Soloviev DM (2020) Oil pollution in the Northern Red Sea: a threat to the marine environment and tourism development. In: Elbeih SF, Negm AM, Kostianoy A (eds) Environmental remote sensing in Egypt. Springer Nature Switzerland AG, Cham, pp 329–362
35. Kostianoy AG (2021) Oil pollution: the Baltic sea. In: Fath BD, Jorgensen SE (eds) Environmental management handbook, 2nd ed. Managing water resources and hydrological systems vol 4. Taylor and Francis, CRC Press, pp 349–368. https://doi.org/10.1201/9781003045045-37
36. Kostianoy AG, Ambjörn C, Solovyov DM (2014a) Seatrack web—a numerical tool for environmental risk assessment in the Baltic sea. In: Kostianoy AG, Lavrova OYu (eds) Oil pollution in the Baltic sea, vol 27. Springer, Berlin, Heidelberg, New York, pp 185–220
37. Kostianoy AG, Bulycheva EV, Semenov AV, Krainyukov AV (2015) Satellite monitoring systems for shipping, and offshore oil and gas industry in the Baltic Sea. Transp Telecommun 16(2):117–126
38. Kostianoy AG, Carpenter A (2018) History, sources and volumes of oil pollution in the Mediterranean sea. In: Carpenter A, Kostianoy AG (eds) Oil pollution in the Mediterranean sea: Part I—the international context. Springer International Publishing AG, Cham, Switzerland, pp 9–31
39. Kostianoy AG, Kostianaia EA, Soloviev DM (2020) Oil pollution in the Mediterranean waters of Egypt. In: Elbeih SF, Negm AM, Kostianoy A (eds) Environmental remote sensing in Egypt. Springer Nature Switzerland AG, Cham, pp 305–328
40. Kostianoy AG, Lavrova OYu (eds) (2014a) Oil pollution in the Baltic sea. In: The handbook of environmental chemistry, vol 27. Springer, Berlin, Heidelberg, New York, p 268
41. Kostianoy AG, Lavrova OYu (2014b) Conclusions. In: Kostianoy AG, Lavrova OYu (eds) Oil pollution in the Baltic sea, vol 27. Springer, Berlin, Heidelberg, New York, pp 249–264
42. Kostianoy AG, Lavrova OYu (2014c) Introduction. In: Kostianoy AG, Lavrova OYu (eds) Oil pollution in the Baltic sea, vol 27. Springer, Berlin, Heidelberg, New York, pp 1–14
43. Kostianoy AG, Lavrova OYu, Mityagina MI, Solovyov DM, Lebedev SA (2014b) Satellite monitoring of oil pollution in the Southeastern Baltic sea. In: Kostianoy AG, Lavrova OYu (eds) Oil pollution in the Baltic sea. Springer, Berlin, Heidelberg, New York, vol 27, pp 125–154
44. Kostianoy AG, Lavrova OYu, Solovyov DM (2014) Oil pollution in coastal waters of Nigeria. In: Barale V, Gade M (eds) Remote sensing of the African Seas. Springer, New York, Heidelberg, Dordrecht, London, pp 149–165
45. Kostianoy AG, Lebedev SA, Litovchenko KTs, Stanichny SV, Pichuzhkina OE (2004) Satellite remote sensing of oil spill pollution in the southeastern Baltic Sea. Gayana 68(2), Part 2:327–332
46. Kostianoy AG, Litovchenko KTs, Lavrova OYu, Mityagina MI, Bocharova TYu, Lebedev SA, Stanichny SV, Soloviev DM, Sirota AM, Pichuzhkina OE (2006) Operational satellite monitoring of oil spill pollution in the southeastern Baltic Sea: 18 months experience. Environm Res Eng Manage N4(38):70–77
47. Krek E, Kostianoy A, Krek A, Semenov AV (2018) Spatial distribution of oil spills at the sea surface in the Southeastern Baltic Sea according to satellite SAR data. Transp Telecommun 19(4):294–300

48. Krek EV, Krek AV, Kostianoy AG (2021) Chronic oil pollution from vessels and its role in background pollution in the Southeastern Baltic Sea. Rem Sens 13:4307. https://doi.org/10.3390/rs13214307
49. Lavrova OYu, Kostianoy AG (2011) A catastrophic oil spill in the Gulf of Mexico in April–May 2010. In: Izvestiya, atmospheric and oceanic physics, vol 47(9). Pleiades Publishing, Ltd, pp 1114–1118
50. Lavrova OYu, Kostianoy AG, Lebedev SA, Mityagina MI, Ginzburg AI, Sheremet NA (2011) Complex satellite monitoring of the Russian seas. IKI RAN, Moscow, p 470 (in Russian)
51. Lavrova OY, Mityagina MI (2013) Satellite monitoring of oil slicks on the Black Sea surface. In: Izvestiya—Atmospheric and Ocean Physics, vol 49(9), pp 897–912
52. Lavrova OYu, Mityagina MI, Kostianoy AG (2016) Satellite methods of detection and monitoring of marine zones of ecological risks. Space Research Institute, Moscow, p 336 (in Russian)
53. Lavrova OYu, Mityagina MI, Kostianoy AG (2019) Online database "See The Sea" for the Caspian Sea. Ecologica Montenegrina 25:79–90
54. Lavrova OYu, Mityagina MI, Kostianoy AG, Semenov AV (2014) Oil pollution in the southeastern Baltic Sea in 2009–2011. Transp Telecommun 15(4):322–331
55. Lavrova OYu, Mityagina MI, Kostianoy AG, Strochkov M (2017) Satellite monitoring of the Black sea ecological risk areas. Ecologica Montenegrina 14:1–13
56. Lu J (2003) Marine oil spill detection, statistics and mapping with ERS SAR imagery in south-east Asia. Int J Rem Sens 24(15):3013–3032
57. Migliaccio M, Gambardella A, Tranfaglia M (2006) Oil spill observation by means of polarimetric SAR data. In: Proceedings of SEASAR 2006, Frascati, Italy, January 23–26 2006, ESA SP-613, April 2006
58. Mityagina M, Churumov A (2006) Radar backscattering at sea surface covered with oil films. Global Developments in Environmental Earth, pp 783–790
59. Mityagina M, Lavrova O (2015) Satellite monitoring of the Black Sea surface pollution. In: 2015 IEEE international geoscience and remote sensing symposium (IGARSS), Milan, Italy, pp 2291–2294. https://doi.org/10.1109/IGARSS.2015.7326265
60. Mityagina MI, Lavrova OYu (2015) Multi-sensor satellite survey of surface oil pollution in the Caspian Sea. In: Proceedings of SPIE 9638, remote sensing of the ocean, sea ice, coastal waters, and large water regions, p 96380Q. https://doi.org/10.1117/12.2194511
61. Mityagina M, Lavrova O (2016) Satellite survey of inner seas: oil pollution in the Black and Caspian Seas. Rem Sens 8:875. https://doi.org/10.3390/rs8100875
62. Mityagina MI (2019) Assessment of surface oil pollution risks of the southeastern Black Sea based on long-term satellite data. In: Proceedings of SPIE 11150, remote sensing of the ocean, sea ice, coastal waters, and large water regions, p 111501C. https://doi.org/10.1117/12.2532867
63. Mityagina MI, Lavrova OYu, Kostianoy AG (2019) Main pattern of the Caspian Sea surface oil pollution revealed by satellite data. Ecologica Montenegrina 25:91–105
64. Mityagina MI, Lavrova OYu (2020) Oil pollution hotspots on the Caspian Sea surface identified using satellite remote sensing. In: Proceedings of SPIE 11529, remote sensing of the ocean, sea ice, coastal waters, and large water regions, p 115290L. https://doi.org/10.1117/12.2573501
65. Monin AS, Voitov VI (1984) Black tides. Moscow, "Molodaya Gvardiya", p 160 (in Russian)
66. Oceana (2003) The other side of oil slicks. In: The dumping of hydrocarbons from ships into the seas and oceans of Europe, p 31. http://www.oceana.org/north-america/publications/reports/the-other-side-of-oil-slicks. Accessed 22 May 2012
67. Oceana (2004) The EU fleet and chronic hydrocarbon contamination of the oceans, p 58. http://www.oceana.org/north-america/publications/reports/the-eu-fleet-and-chronic-hydrocarbon-contamination. Accessed 22 May 2012
68. Patin SA (2008) Oil spills and their impact on the marine environment and living resources. VNIRO Publishing, Moscow, p 508 (in Russian)
69. Periáñez R (2020) A Lagrangian oil spill transport model for the Red Sea. Ocean Eng 217:107953. https://doi.org/10.1016/j.oceaneng.2020.107953

70. Redondo JM, Platonov A, Tarquis A (2008) Detection and prediction from SAR multiscale analysis. In: The 2nd international workshop on advances in SAR oceanography from Envisat and ERS missions, SeaSAR 2008, 21–25 January 2008, Rome, Italy
71. Sano EE, Matricardi EAT, Camargo FF (2020) State-of-the-art of radar remote sensing: fundamentals, sensors, image processing, and applications. Revista Brasileira de Cartografia 72:1484–1508. https://doi.org/10.14393/rbcv72nespecial50anos-56568
72. Shcherbak SS, Lavrova OY, Mityagina MI, Bocharova TY, Krovotyntsev VA, Ostrovskii AG (2008) Multisensor satellite monitoring of seawater state and oil pollution in the northeastern coastal zone of the Black Sea. Int J Rem Sens 29(21):6331–6345.https://doi.org/10.1080/01431160802175470
73. Shi L, Ivanov AYu, He M-X, Zhao C (2008) Oil spill mapping in the western part of the East China Sea using synthetic aperture radar imagery. Int J Rem Sens 29(21):6315–6329
74. Solberg A, Schistad H, Storvik G, Solberg R, Volden E (1999) Automatic detection of oil spills in ERS SAR images. IEEE Trans Geosci Rem Sens GE-37:1916–1924.4
75. Terleeva NV, Kamagate SA, Ivanov AYu (2012) Oil pollution in the Gulf of Guinea based on satellite radar data. Earth from Space 13:51–56 (in Russian)
76. Topouzelis K, Bernardini A, Ferraro G, Meier-Roux S, Tarchi D (2006) Satellite mapping of oil spills in the Mediterranean Sea. Fresenius Environ Bulletin 15(9A):1009–1014
77. Topouzelis K, Karathanassi V, Pavlakis P, Rokos D (2007) Detection and discrimination between oil spills and look-alike phenomena through neural networks. ISPRS J Photogramm Rem Sens 62(4):264–270. https://doi.org/10.1016/j.isprsjprs.2007.05.003
78. UNESCO (2003) The integrated, strategic design plan for the coastal ocean observations module of the Global Ocean Observing System. GOOS Report n° 125, IOC Information Documents Series N 1183, UNESCO, Paris, p 190
79. Valenzuela GR (1978) Theories for interaction of electromagnetic and oceanic waves—a review. Boundary Layer Meteorol 13:61–75
80. Zhurbas V, Välib G, Kostianoy A, Lavrova O (2019) Hindcast of mesoscale eddy field in the Southeastern Baltic Sea: model data vs satellite imagery. Russ J Earth Sci 19:ES4006. https://doi.org/10.2205/2019ES000672
81. Zodiatis G et al (2018) Numerical modeling of oil pollution in the Eastern Mediterranean Sea. In: Carpenter A, Kostianoy A (eds) Oil pollution in the Mediterranean Sea: Part I. The handbook of environmental chemistry, vol 83. Springer, Cham. https://doi.org/10.1007/698_2017_131